Materials International
Open-Access Journal (ISSN: 2668-5728)

Article
Volume 7, Issue 4, 2025, 40
https://doi.org/10.33263/Materials74.040

Experimental and Theoretical Investigation of a Naphthyl-Based Saline Compound as a Multi-Anion Chemosensor

Gershon Amenuvor [1], Issah Yahaya [2,*], Caroline Rosemyya Kwawu [1], Faustina Dufie Wireko-Manu [3], Bernard Konadu Amoah [4], Evans Adei [1], Shuraif Abdul-Rafiu [1], Benjamin Gyedu Akonor [1]

[1] Department of Chemistry, Kwame Nkrumah University of Science and Technology; gershon.amenuvor@knust.edu.gh (G.A.); kwawucaroline@knust.edu.gh (C.R.K.); eadei.cos@knust.edu.gh (E.A.); sabdulrafiu2@st.knust.edu.gh (S.A.-R.); bgakonor@st.knust.edu.gh (B.G.A.);
[2] Department of Chemical Sciences, School of Sciences, University of Energy and Natural Resources; issah.yahaya@uenr.edu.gh (I.Y.);
[3] Department of Food Science and Technology, Kwame Nkrumah University of Science and Technology; fdwireko-manu.cos@knust.edu.gh (F.D.W.M.);
[4] Department of Geological Engineering, Kwame Nkrumah University of Science and Technology; bernardkamoah@knust.edu.gh (B.K.A.);
* Correspondence: issah.yahaya@uenr.edu.gh (I.Y.);

Received: 24.04.2025; Accepted: 27.07.2025; Published: 10.12.2025

Abstract: Ion sensing is crucial in industries for quality control of products such as food and water. In this work, a dinaphthyl-based saline compound (DiNa) was used as a chemosensor for anion detection in solution. The selectivity and sensitivity of DiNa for the anions (CN^-, F^-, I^-, Br^-, Cl^-, AcO^-, NO_3^-, and ClO_4^-) were determined with UV-Vis titration and it was found that DiNa can be employed for the detection of CN^-, F^-, and I^-, which showed a strong interaction with the probe in the presence of other ions as competitors. Colorimetric and fluorescence changes visible to the naked eye and under 365 nm UV light were observed upon addition of CN^-, F^-, and I^- to the solution of DiNa in EtOH/H_2O (9:1, v/v) binary solvent. The chemosensor showed no chromogenic and fluorescence responses for other competing anions (Br^-, Cl^-, AcO^-, NO_3^-, and ClO_4^-). The mechanisms for the signaling of the anions have been found to be by H-bonding, then followed by deprotonation, and by addition to the imine (–C=N-) bond. The sensing mechanisms of the chemosensor were verified by DFT and TD−DFT calculations to support the experimental results. The results of this research have the potential to guide subsequent designs of probes of similar functionalities for selective anion detection. Finally, the probe could be utilized in the detection of CN^-, F^-, and I^- in samples in solution.

Keywords: multi-anion detection; chemosensor; DFT and TD-DFT calculations; deprotonation; selectivity.

1. Introduction

In recent decades, there has been significant interest in anion detection across various applications, including physiological and environmental monitoring [1,2]. Due to increasing industrialization, several anions are generated as part of industrial pollutants. For instance, cyanide anions, which are extremely toxic to humans and other living organisms [3-5], are predominant wastes produced from gold mining, electroplating, and metallurgy industries [6]. It has been reported that gold mining and electroplating industries consume about 1.1 million

tons of cyanide annually [7]. Cyanide from industrial waste effluents eventually enters the aquatic environment, thereby poisoning organisms through the food chain [8]. The health implications of other anions, such as the halides, cannot be overemphasized. Fluorides, though essential in human health, can cause several health conditions, including risk of fluorosis in children, kidney diseases, and cancer [9, 10]. In addition to its effect on human health, excess fluoride in plants is known to retard plant growth and reduce yield [11,12]. The significance of iodine in maintaining human health cannot be overestimated, and eliminating its presence from our diet would invite illnesses such as goiter. However, an excess of it can be detrimental to some individuals. Over the years, various kinds of molecules that contain acidic protons, such as -NH and -OH, and the imine moiety (-C=N-) have been studied for their ability to sense these anions (CN^-, F^-, and I^-) using a sensor [13-18]. Some of these molecules are able to sense single anions, while others could detect multiple anions. For instance, Uahengo and co-workers used naphthyl-based hydrazone receptors to detect cyanide, hydroxide, and other anions in real time, naked-eye, from tap water [14]. Similarly, Yahaya *et al*. employed coumarin-thiophene amides, sulfonamide, and urea derivatives to sense multiple singly charged anions, including cyanide, chloride, bromide, acetate, and several other anions [16]. The mechanisms of ion sensing are thought to vary depending on the receptor's functional groups and the type of anion. In this work, we studied the interactions of cyanide, fluoride, iodide, and bromide ions with a dinaphthyl-based probe and performed DFT calculations on the interactions of cyanide and fluoride with the probe.

2. Materials and Methods

2.1. Chemicals and general instrumentation.

All chemicals were of analytical grade and used without further purification. The compounds, 2-Hydroxy-1-naphthaldehyde and o-phenylenediamine, were obtained from Sigma Aldrich. All solvents were dried on molecular sieves prior to use. The infrared (IR) spectra were recorded on a Bruker Platinum ALPHA ATR FT-IR Spectrometer in the region of 4000–400 cm^{-1}. The ^1H NMR spectra were recorded on a Bruker 500 MHz high-temperature superconducting NMR spectrometer using $CDCl_3$ as the internal standard. All UV-Visible spectrometric data were acquired using a SHIMADZU UVmin-1800 UV-Vis Spectrophotometer and glass cuvettes (1 cm x 1 cm x 4.5 cm).

2.2. Synthesis of probe DiNa.

The synthesis of DiNa was performed in a similar manner as described in the literature [16]. Compound, 2-Hydroxy-1-naphthaldehyde (0.2 g, 1.16 mmol), was dissolved in 15.0 mL of ethanol, followed by the addition of o-phenylenediamine (0.062 g, 0.58 mmol), as depicted in Scheme 1. The solution was stirred and refluxed for 4 h. The solution was cooled, the precipitate filtered, washed with cold ethanol, and dried in vacuo to obtain a bright yellow solid. Yield: 0.20 g (85.71%). ^1H NMR ($CDCl_3$): δ 7.27 (d, benzene-CH, 2H), 7.32 (d, benzene-CH, 2H), 7.36 (d, benzene-CH, 4H), 7.38 (d, benzene-CH, 2H), 7.45 (d, benzene-CH, 2H), 7.69 (d, benzene-CH, 2H), 7.77 (d, benzene-CH, 2H), 8.10 (d, benzene-CH, 2H), 9.42 (s, N=CH, 2H), 15.03 (s, Ar-OH, 2H). IR (ATR): 1150 (C-O stretch), 3047 (Aromatic C-H stretch), 1650 (C=N stretch), 1600 (C=C stretch).

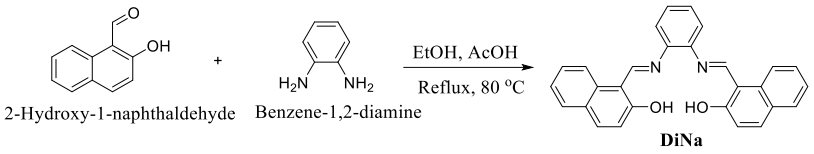

Scheme 1. Synthesis of probe DiNa.

2.3. Spectroscopic measurements of DiNa toward various anions.

Titrant (DiNa) solution was freshly prepared with a concentration of 30 μM in EtOH/H_2O (9:1, v/v). To study the wide-spectrum application of the sensor DiNa, eight different anions (CN^-, F^-, I^-, Br^-, Cl^-, AcO^-, NO_3^-, and ClO_4^-) were interacted with it, and the various mixtures were examined by UV-Vis spectroscopy. All measurements were completed in UV quartz cuvettes (path length, l = 1 cm) at room temperature. The UV-Vis analysis was initially scanned from 200 to 800 nm and was later set at 200 to 300 nm as the maximum absorption for all anion interactions with the probe occurs within this region.

2.4. Computational methods for sensing mechanism of the anions.

The density functional theory (DFT) at the B3LYP/6-311++G(d,p) level was used to optimize the interaction mechanism of the anions sensed by DiNa [19–22].

The hybrid functional can be used to investigate spectroscopic parameters and elucidate the mechanisms of anion interactions in various chemosensors [15,16,23,24]. The optimized molecular geometries were characterized as true minima by full harmonic vibrational frequency calculations. Solvent effects of THF, H_2O, and DMSO were taken into account by full optimization of the gas phase structures through the polarizable continuum model (PCM) [25-27]. At the same level, the electronic absorption spectra were acquired using time-dependent DFT (TD-DFT) [28,29]. The Gaussian 09 software was utilized for all DFT and TD-DFT computations [30]. Additional estimated free energies are relative energies, since the reactant energy is set to zero [31].

3. Results and Discussion

3.1. Interaction of DiNa toward various anions.

The probe, DiNa, demonstrates distinct UV-visible absorption changes in response to the various anions (CN^-, F^-, I^-, Br^-, Cl^-, AcO^-, NO_3^-, and ClO_4^-). The optical properties of DiNa, measured as absorbance at different wavelengths, reveal selective interactions with these anions, as evidenced by wavelength shifts and intensity variations.

Differences in absorption intensities and wavelength shifts, including bathochromic shifts and minor signals (minor peaks), point to the extent of DiNa's interaction with these anions. Acetate absorbs moderately across three key wavelengths, with slight variations in the 240-250 nm range (Figure 1). These secondary peaks may indicate a weaker binding interaction between acetate and DiNa, with fewer π–π* or n–π* transitions at these wavelengths (Figure 1).

Iodide shows a strong binding affinity for DiNa, as reflected by the high absorbance, particularly at 236 nm, and a distinct band at 242 nm (Figure 2). The intensity suggests significant electronic interaction or charge-transfer processes, which may indicate a strong interaction between iodide and the receptor [32].

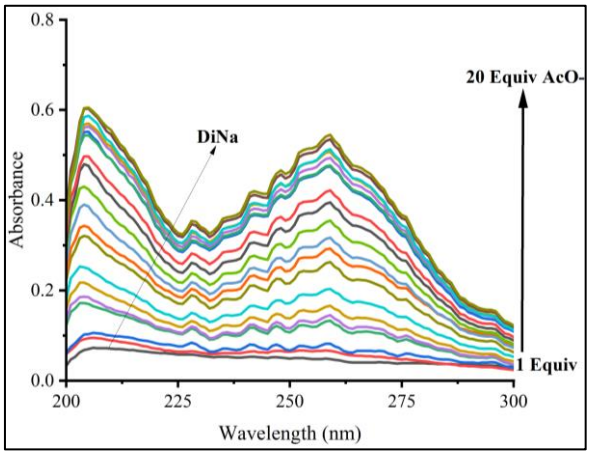

Figure 1. UV–visible titration investigation with gradual addition of acetate ion (10 mM) against the probe DiNa (30 μM).

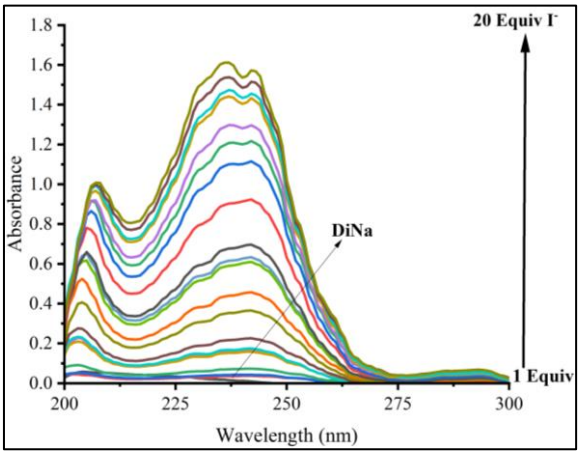

Figure 2. UV–visible titration investigation with gradual addition of iodide ion (10 mM) against the probe DiNa (30 μM).

Bromide exhibits a small interaction, with an isolated peak at 209 nm (Figure 3). The relatively high absorbance observed with bromide ions indicates moderate selectivity of the probe for bromide, though not as strong as for iodide [33]. The absence of multiple peaks suggests simpler binding dynamics compared to other ions. Chloride shows intermediate binding, with noticeable absorption at three distinct wavelengths (Figure 4). The band at 259 nm is relatively strong, suggesting charge transfer, while the additional absorptions may indicate structural interactions between DiNa and chloride.

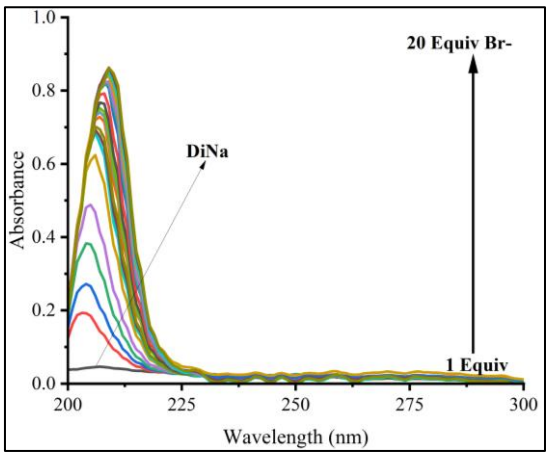

Figure 3. UV–visible titration investigation with gradual addition of bromide ion (10 mM) against the probe DiNa (30 μM).

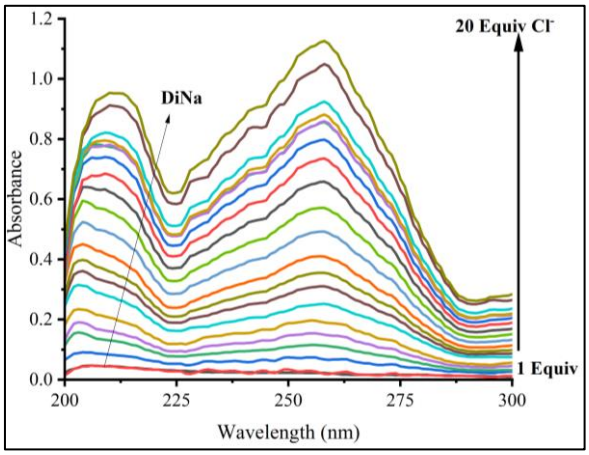

Figure 4. UV–visible titration investigation with gradual addition of chloride ion (10 mM) against the probe DiNa (30 μM).

Fluoride exhibits a strong interaction with DiNa, with the maximum absorption at 227 nm, showing a bathochromic shift. The high intensity at this wavelength may suggest significant hydrogen bonding or a stronger binding mechanism [34] compared to that of other halide ions (Figure 5). Nitrate has a weak interaction with DiNa, as indicated by the low absorbance. This suggests either a low binding affinity or minimal charge-transfer interactions between DiNa and the nitrate ion (Figure 6).

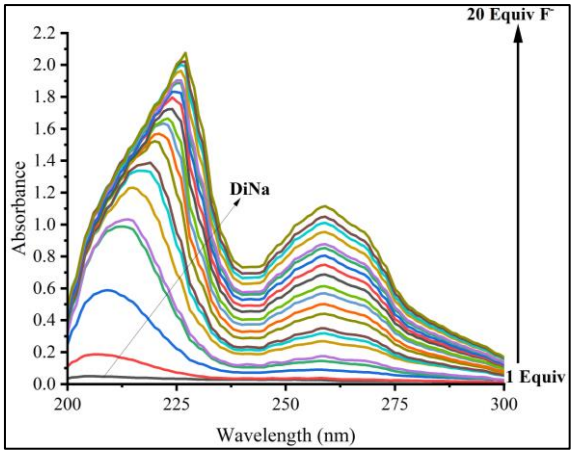

Figure 5. UV–visible titration investigation with gradual addition of fluoride ion (10 mM) against the probe DiNa (30 μM).

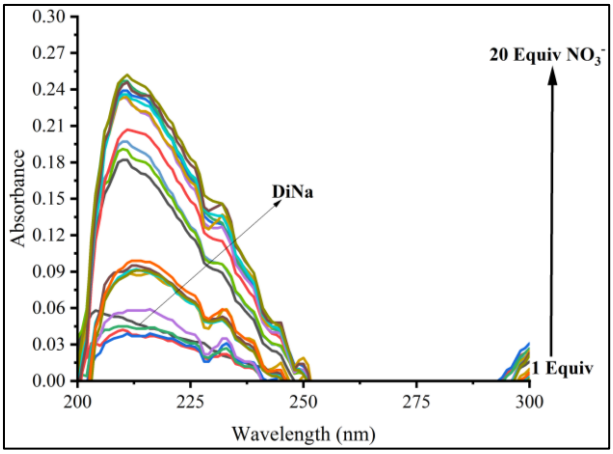

Figure 6. UV–visible titration investigation with gradual addition of nitrate ion (10 mM) against the probe DiNa (30 μM).

Cyanide shows the strongest interaction with DiNa among the ions tested, with a significant bathochromic shift and an absorption intensity of 2.444 at 230 nm (Figure 7). The shift indicates a strong interaction of the CN- with the probe, possibly through π−acceptor binding, or formation of covalent-like bonds with DiNa [35]. Chlorate indicates the weakest interaction with DiNa, with very low absorbance across the spectrum. The multiple weak peaks imply only minor interaction, suggesting a weak selectivity of DiNa towards chlorate (Figure 8).

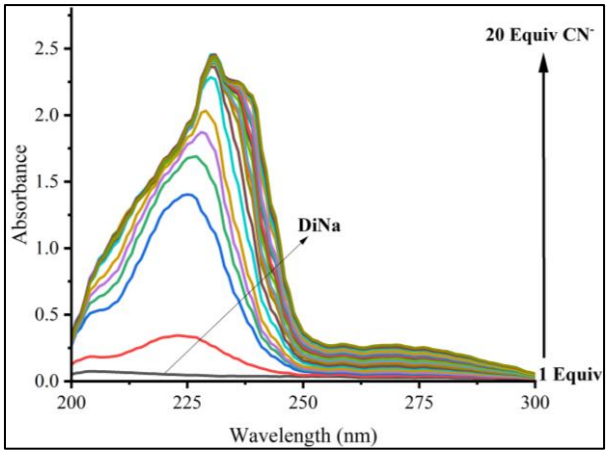

Figure 7. UV–visible titration investigation with gradual addition of cyanide ion (10 mM) against the probe DiNa (30 μM).

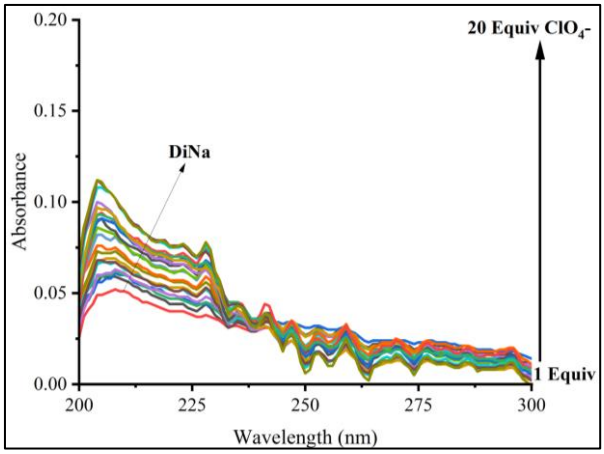

Figure 8. UV–visible titration investigation with gradual addition of chlorate ion (10 mM) against the probe DiNa (30 μM).

3.2. Selectivity of the probe DiNa towards various anions.

We have also studied the extent to which different anions can interfere with the probe. The selectivity profile of DiNa towards the anions (CN^-, F^-, I^-, Br^-, Cl^-, AcO^-, NO_3^-, and ClO_4^-) reveals varied interaction strengths (Figure 9). Among the anions investigated, CN^- and F^- show the strongest interaction, making them the most selective targets of the probe. However**,** I^- and Cl^- exhibit moderate interactions, though weaker than cyanide and fluoride. The other anions, Br^-, AcO^-, and NO_3^- show poor binding, with bromide and nitrate having particularly weak affinities. Interaction of ClO_4^- with the probe did not result in any significant changes in the absorption, which demonstrates minimal interaction and selectivity towards this ion. Overall, DiNa exhibits high selectivity for small, highly electronegative, or nucleophilic anions such as F− and CN−, while showing weaker responses to larger or less polarizable anions such as Br^- and ClO_4^-.

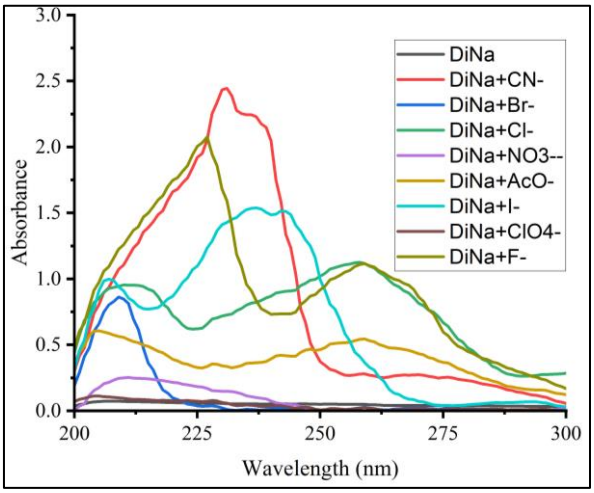

Figure 9. UV–vis absorption spectrum of DiNa in the presence of variety of anions for Selectivity and interference studies.

3.3. Chromogenic reaction to the competing ions.

20 equiv of each of the anions (CN−, F−, I−, Br−, Cl−, AcO−, NO_3−, and ClO_4−) were added to the chemosensor DiNa to induce a chromogenic response. But the only ones that responded significantly were CN−, F−, and I−. No coloration change was seen for the other competing anions (Br−, Cl−, AcO−, NO_3−, and ClO_4−), as Figure 10 illustrates.

Under the ambient light, as depicted in Figure 10, the probe DiNa showed a change in coloration from light brown to colorless for CN^-, F^-, and I^-, but the coloration remains unchanged with the remaining anions (Br^-, Cl^-, AcO^-, NO_3^-, and ClO_4^-).

Under the 365 nm UV light, the chemosensor DiNa showed a change in coloration from light brown to deep greenish for CN^-, F^-, and I^-, but the coloration with the remaining anions (Br^-, Cl^-, AcO^-, NO_3^-, and ClO_4^-) was blue-black (Figure 11).

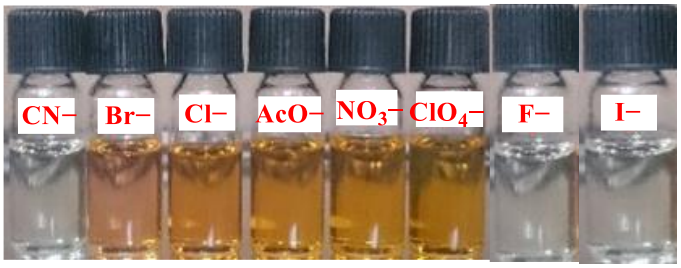

Figure 10. Colorimetric and fluorescence changes of DiNa with the addition of 20 equiv of the anions under ambient light.

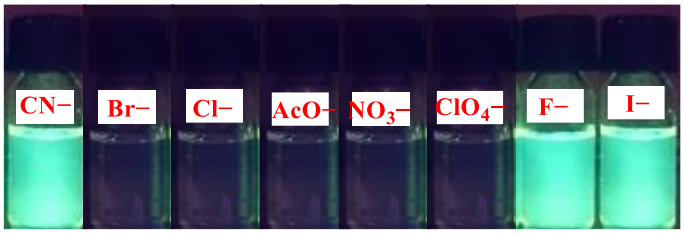

Figure 11. Colorimetric and fluorescence changes of DiNa with the addition of 20 equiv of the anions under 365 nm UV light.

3.4. Sensing mechanisms.

In 2020, Yahaya *et al*. published a paper detailing various mechanisms in signaling anions, which included H-bonding, di-deprotonation, and de-monosulfonation [16]. Again, In

2024. Kiran *et al*. [35] reported a similar deprotonation approach in the recognition of cyanide in aqueous medium with a solid-state. This research is aligned with these findings. This is due to the reasoning that our probe may show H-bonding, di-deprotonation, and also a nucleophilic attack on the imine (-C=N-) part of our chemosensor (Scheme 2). Therefore, we probed and identified the sensing mechanisms involved in the recognition of the signaled anions (CN−, F−, and I−) that interact with the chemosensor DiNa. The sensing mechanism for the anions (CN^-, F^-, and I^-) using DiNa via the anions' initial hydrogen bonding with the chemosensor, which ensues by deprotonation, and then, anion addition to imine carbon is shown in Scheme 2. These mechanisms have been confirmed by using DFT calculations.

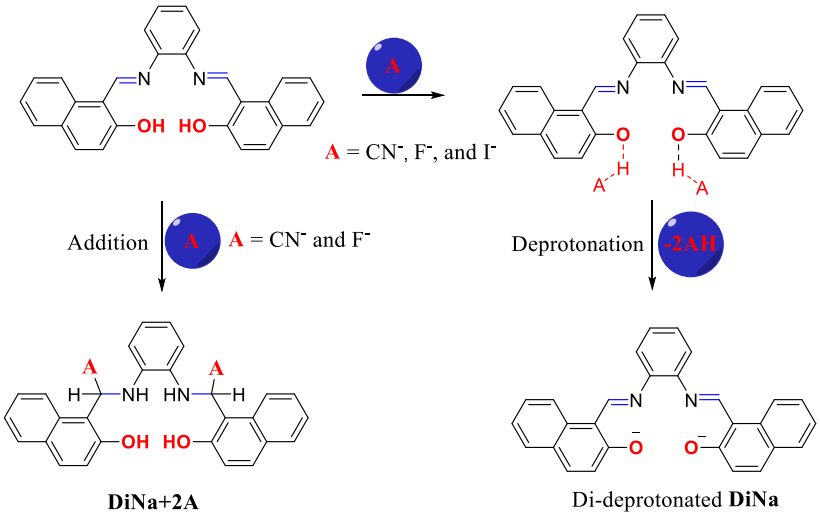

Scheme 2. Proposed binding mechanisms of chemosensor DiNa with CN^-, F^-, and I^- in a binary solution ($EtOH/H_2O$:9/1 v/v).

3.5. DFT Calculations and computational details for sensing mechanism of the anions.

Initially, four different reaction pathways were proposed based on the literature [16,36-38] for the interaction mechanism of DiNa with anions, as illustrated in Scheme S1 of the Supplementary information. Pathway one (PATH 1) illustrates a process where the anion forms a hydrogen bond with the −OH on DiNa and subsequently deprotonates the −OH group to form the final product (P1). In the second path, the anion would first attack the carbon bonded directly to the −OH. This condition makes the −OH a good leaving group and hence, would undergo substitution by the anion to form P2. For PATH 3, there is first an intermolecular transfer of a proton from the −OH group to the nitrogen in DiNa through hydrogen bonding, and this creates the condition for the anion to attack the imine carbon to form the final product (P3). In the last proposed pathway (PATH 4), the anion attacks the nitrogen of DiNa, breaking the pi-bond between the −C=N−, to form product P4.

Table 1. Calculated reaction energies of products from the interaction between DiNa and CN^- for the different proposed pathways.

Product	Reaction energy
P1	7.49
P2	64.73
P3	−14.80
P4	62.01

The reaction energies of the various products generated for all four pathways for CN^- interaction with the probe are shown in Table 1. From these results, only the reaction energy of the product (P3) along PATH 3 is exergonic with a reaction energy of −14.80 kcal/mol and

hence thermodynamically feasible. On the basis of these findings, the remaining pathways (P1, P2, and P4) were eliminated for the sensing mechanism of CN^- by DiNa since their final products will not be stable.

In order to further investigate the sensing mechanism of CN^- by DiNa along PATH 3, the calculated Gibbs free energy profile is shown in Figure 12. The reaction of DiNa to afford P3 is a four-step process involving intramolecular proton abstraction reaction steps to generate the corresponding intermediates that further undergo a nucleophilic attack by the anion (CN^-) to form P3. As shown in Figure 12, the formation of intermediate INT3A proceeds via transition state TS3A, with an activation energy of 3.5 kcal/mol. Due to the symmetrical nature of DiNa, the second step is also an intramolecular proton abstraction through TS3B to form INT3B with a barrier of 2.4 kcal/mol. However, the third step is when the first CN^- comes in, and this step is a barrierless process with an activation energy of –12.6 kcal/mol through TS3C to form INT3C. The final step then proceeds via TS3D to produce P3 with a high activation barrier of 41.1 kcal/mol.

In Table 2, the effect of different solvents (DMSO, H_2O, and THF) on the energetic trends was explored. From the results, the various solvents are observed to have an overall effect in reducing both the activation barrier and reaction energies in the order of H_2O > DMSO > THF. However, compared to gas phase calculations, the energetic trends were consistent with those for all considered solvents (DMSO, H_2O, and THF).

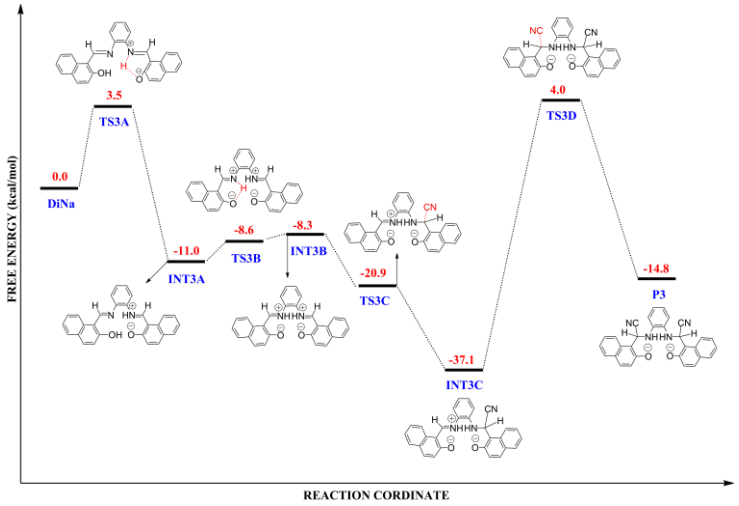

Figure 12. Free energy profile of the proposed sensing mechanism by DiNa for CN^- at the B3LYP/6-311++G (d, p) level of theory. All free energies are in kcal/mol.

Table 2. Activation and reaction energies of transition states, intermediates, and products for the interaction between DiNa and CN^- in different solvents at the B3LYP/6-311++G (d, p) level of theory. All free energies are in kcal/mol.

Solvent	TS3A	INT3A	TS3B	INT3B	TS3C	INT3C	TS3D	P3
DMSO	−0.08	−12.32	–	−7.49	–	−9.81	–	−8.87
THF	0.47	−12.06	–	−10.89	–	−12.46	20.83	−8.15
H_2O	−0.12	−12.35	–	−7.25	–	−9.61	17.83	−8.97
Gas phase	3.48	−10.96	2.40	−8.25	−12.65	−37.11	41.07	−14.80

Moreover, changes in natural charges and frontier orbital analysis may be used to explain changes in the experimental absorption spectra after proton transfer and DiNa's interaction with CN^-. The computed natural charges on the non-ring carbon, oxygen, and nitrogen atoms are shown in Figure 13. The natural charges on C, O, and N atoms of the ground state of DiNa change from 0.16e, −0.68e, and −0.52e to −0.16e, −0.82e, and −0.69e, respectively, after interaction with the CN^-. This observed increase in negative charges on C,

O, and N atoms after the intramolecular proton transfer and DiNa interaction with CN^- processes will cause an increase in the intramolecular charge transfer for the molecule [15].

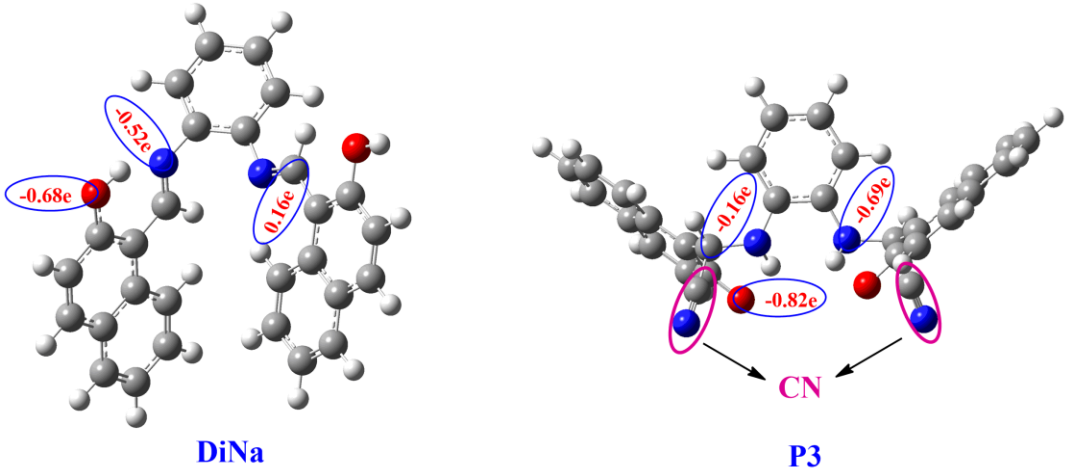

Figure 13. The optimized structures of DiNa and P3 and natural charges on C, O, and N atoms at the B3LYP/6-311++G (d, p) level of theory. Blue: *N*; Gray: *C*; Red: O; White: *H*.

The frontier orbitals HOMO and LUMO energies and the gap between HOMO and LUMO (ΔE) for DiNa and P3 are given in Figure 14. The ΔE value decreases by 0.36 eV upon interaction with the CN^- ion, and this leads to a bathochromic shift in the absorption spectra of P3. For DiNa, the electron density is observed to spread over the entire molecule in both the HOMO and LUMO. For P3, the electron density on HOMO shifted towards one of the naphthol and the benzene moieties, whereas LUMO experiences electron cloud shift towards only the naphthol part. These indicate that there is an increase in the intramolecular charge transition after the interaction with the CN^-. These observations are consistent with the experimental findings (Figure 7).

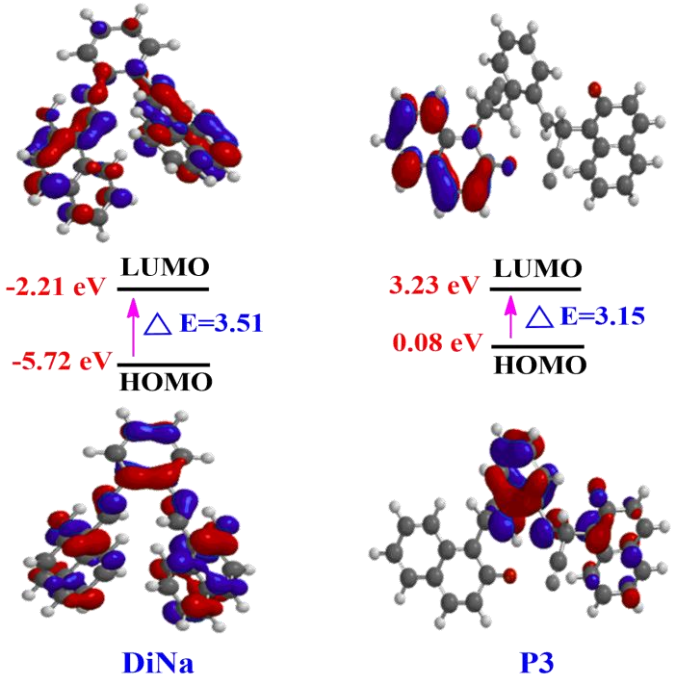

Figure 14. The frontier orbitals (*HOMO* and *LUMO*), their energies, and the energy gap (ΔE) of DiNa and P3 (DiNa + CN^-).

The computed absorption maximum wavelengths coupled with the absolute CI coefficients and related oscillator strengths (*f*) for both DiNa and P3 (DiNa + CN^-) are given

in Table 3. The absorption peaks at 421 nm with the oscillator intensity of DiNa's computed first singlet transition (S0 → S1) 0.1451, whereas that of DiNa + CN^- is 469 nm for the absorption maxima and 0.0012 for its oscillator strength. The observed bathochromic shifts can be associated with increased intramolecular charge transfer, due to intramolecular proton transfer and DiNa interaction with CN−, as previously analyzed from other parameters [13].

Table 3. Calculated electronic excitation energies (nm), integrating oscillator strengths (*f*), composition, and low-lying singlet excited state CI coefficients for DiNa and P3.

	Transition	λmax (nm)	*f*	Composition	CI (%)
DiNa	$S_0 \rightarrow S_1$	421	0.1451	HOMO → LUMO	3.75
				HOMO+2 → LUMO	92.84
P3	$S_0 \rightarrow S_1$	469	0.0012	HOMO → LUMO	47.10
				HOMO+1 → LUMO-1	52.30

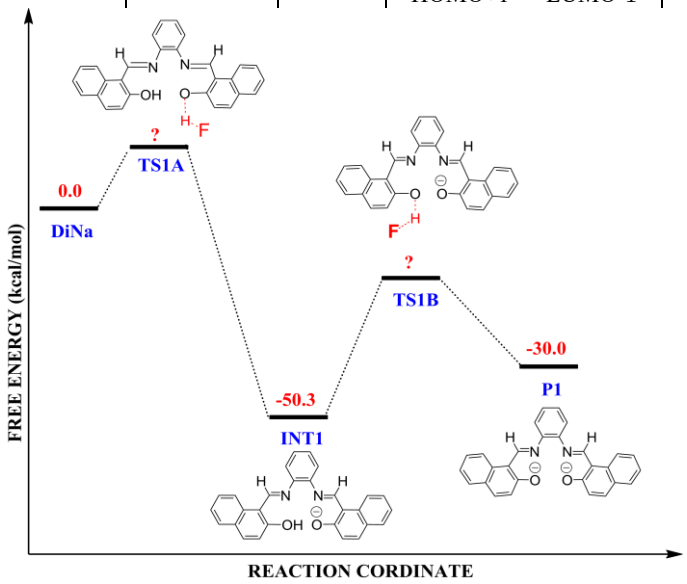

Figure 15. Free energy profile of the proposed sensing mechanism by DiNa for F^- at the B3LYP/6-311++G (d, p) level of theory. All free energies are in kcal/mol.

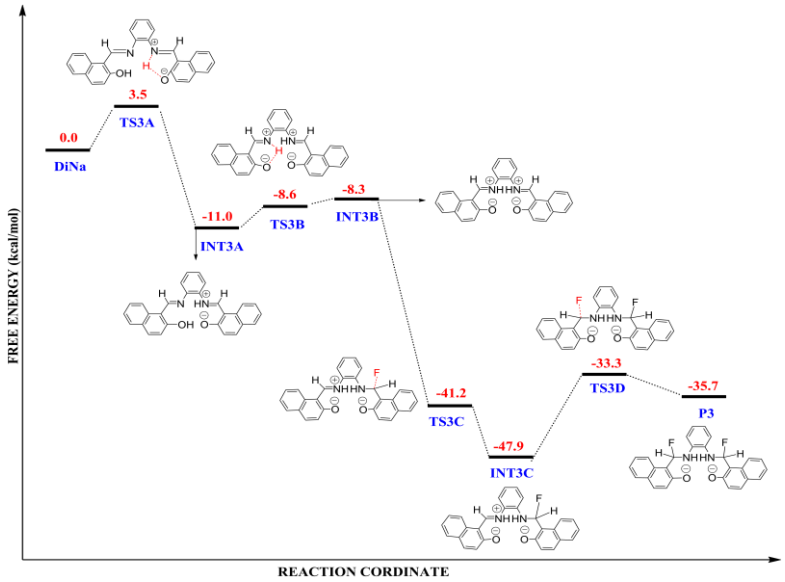

Figure 16. Free energy profile for PATH 3 of the sensing mechanism for F− by DiNa at the B3LYP/6-311++G (d, p) level of theory. All free energies are in kcal/mol.

Contrary to the observations made for CN^-, where only the PATH 3 was feasible, both PATH 1 and PATH 3 are probable routes for the sensing of F^- by DiNa. The results indicate that the interaction of F^- with DiNa through PATH 3 has relatively lower activation and

reaction energies (Figure 14) compared to that of CN^-. This means that, should the mechanism go through the PATH 3, there will be a competition in selectivity between F^- and CN^- ions, with the F^- having a slight edge over the CN^-.

As shown in Figure 15, the reaction of F^- with the probe along PATH 1 produces both a stable intermediate and product. However, no data were obtained for its transition states (TS1A and TS1B) after exhaustive search.

Nonetheless, based on these results and other experimental parameters, it can be inferred that the most probable mechanism for the F^- interaction with DiNa is through the PATH 1, which results in a product with the lowest energy of -35.7 kcal/mol, and this also becomes the likely mechanism for all the other halides.

To investigate competition between the two most favored anions (CN^- and F^-) for the chemosensor DiNa, we calculated their interaction energies with the DiNa, and the results are shown in Table 4.

Table 4. Calculated interaction energies (*Int*) for DiNa with different anions (CN^- and F^-).

Anions	**E_{int} (kcal/mol)**	
	Single Int	*Double Int*
CN^-	28.86	−22.31
$F-$	39.64	−12.21

The interaction energies were calculated by using the formula: $E_{int} = E_{DiNa} + E_{anion} - E_{P3}$ [38,39], where E_{int}, E_{DiNa}, E_{anion}, and E_{P3} represent the interaction energies, the energy of DiNa, the energy of anion, and the energy of P3, respectively. The findings indicate that the interaction energy between DiNa and F^- is the largest for both the first and second interactions of the anion with DiNa. The large interaction energies for F^-, as compared to CN^-, indicate that the DiNa has a high selectivity towards F^-, and that the other anions have little to no effect on DiNa.

4. Conclusions

In this study, a Schiff base molecule, DiNa, has shown interaction with a wide range of anions in solution. Cyanide, fluoride, and iodide ions exhibit highly selective, sensitive, and very fast responses to the sensor. The interactions of the probe with the signaled anions (CN^-, F^-, and I^-) indicate two main mechanisms (a general deprotonation process and an addition reaction). Furthermore, the chemosensor could detect and distinguish CN^-, F^-, and I^- even in the sample containing all the other competing anions. DFT calculations reveal that the thermodynamically favorable pathway for cyanide interaction with the probe involves reduction of the imine bond, with cyanide binding to the imine carbon atom. Fluoride detection is shown to follow the same mechanisms as cyanide and pathway 1, in which fluoride deprotonates the hydroxy group. Energetics revealed that both cyanide and fluoride ions prefer the imine carbon, leading to a reduction in the imine double bond. An alternative mechanism for fluoride binding to the probe is via deprotonation of the hydroxy group on the naphthyl moiety. This resulted in a relative free energy of -35.7 kcal for the product compared to -30 kcal calculated when binding occurred through the imine carbon. Finally, the chemosensor DiNa showed fluorescence and colorimetric changes in the ambient and UV light (365 nm). Therefore, it is expected that this chemosensor could be employed as a sensor for immediate recognition of CN^-, F^-, and I^- in solution.

Author Contributions

Conceptualization, I. Y. and G.A.; methodology, I. Y., G. A., F. D. W-M, and B. K. A.; software, E. A., B. G. A., and S. A-R.; validation, I. Y., G. A., C. R. K., E. A., B. G. A., and S. A-R.; formal analysis, I. Y., G. A., C. R. K., E. A., B. G. A., and S. A-R.; investigation, I. Y., G. A., C. R. K., E. A., B. G. A., and S. A-R.; resources, G. A., I. Y., F. D. W-M, and B. K. A.; data curation, E. A., B. G. A., and S. A-R.; writing—original draft preparation, I. Y., G. A., C. R. K.; writing—review and editing, I. Y. and C. R. K.; visualization, B. K. A., E. A., and C. R. K.; supervision, I. Y. and G.A.; project administration, I. Y. and G.A.; funding acquisition, G.A. All authors have read and agreed to the published version of the manuscript.

Data Availability Statement

No new data were created or analyzed in this study. Data sharing is not applicable.

Funding

This research received no external funding.

Acknowledgments

The authors are grateful to the KNUST Research Fund (KReF) for their financial support toward this project.

Conflicts of Interest

The authors declare no conflict of interest.

References

1. Dutta, S.; Sahana, A. Ratiometric fluorescence-based and chromogenic sensors for the detection of fluoride ions and their application in real samples. *Anal. Methods* **2024**, *16*, 344–370, https://doi.org/10.1039/D3AY01840G.
2. Majeed, S.; Waseem, M. T.; Khan, G. S.; Junaid, H. M.; Imran, M.; Nawazish, S.; Khan, T. A.; Mahmood, T.; Shahzad, S. A. Development of AIEE Active Fluorescent and Colorimetric Probe for the Solid, Solution, and Vapor Phase Detection of Cyanide: Smartphone and Food Applications. *Analyst* **2022**, *147*, 3885–3893, https://doi.org/10.1039/D2AN00937D.
3. Goyal, H.; Annan, I.; Ahluwalia, D.; Bag, A.; Gupta, R. Discriminative 'Turn-on' Detection of Al^{3+} and Ga^{3+} Ions as Well as Aspartic Acid by Two Fluorescent Chemosensors. *Sensors* **2023**, *23*, 1798, https://doi.org/10.3390/s23041798.
4. Zhao, H.-W.; Wu, G.; Sun, X.-Y.; Chao, J.-B.; Li, Y.; Jiang, L.; Han, H. A highly selective and ratiometric molecular probe for cyanide sensing based on a phenothiazine-hemicyanine dye. *J. Lumin.* **2018**, *201*, 474–478, https://doi.org/10.1016/j.jlumin.2018.05.021.
5. Li, L.; Zan, M.; Qie, X.; Miao, P.; Yue, J.; Chang, Z.; Wang, Z.; Bai, F.-Q.; Zhang, H.-X.; Ferri, J.K. A highly selective fluorescent probe for cyanide ion and its detection mechanism from theoretical calculations. *Talanta* **2018**, *185*, 1–6, https://doi.org/10.1016/j.talanta.2018.03.013.
6. Jaszczak, E.; Polkowska, Ż.; Narkowicz, S.; Namieśnik, J. Cyanides in the environment—analysis—problems and challenges. *Environ. Sci. Pollut. Res*. **2017**, *24*, 15929–15948, https://doi.org/10.1007/s11356-017-9081-7.
7. Wu, Y.; Ding, W.-M.; Li, J.; Guo, G.; Zhang, S.-Z.; Jia, H.-R.; Sun, Y.-X. A Highly Selective Turn-on Fluorescent and Naked-eye Colourimetric Dual-channel Probe for Cyanide Anions Detection in Water Samples. *J. Fluoresc.* **2021**, *31*, 437–446, https://doi.org/10.1007/s10895-020-02677-x.

8. Canadian Council of Resource and Environment Ministers (CCREM). Canadian Water Quality Guidelines; Water Quality Branch. Environment Canada: Ottawa, Canada, **1987**.
9. Zalmi, G.A.; Jadhav, S.E.; Mirgane, H.A.; Madje, B.R.; Bhosale, S.V. A Phenolic Schiff Based AIE-Active Quinoxaline-Based Receptor for Selective Sensing of Fluoride Ions. *Chem. Select* **2023**, *8*, e202203380, https://doi.org/10.1002/slct.202203380.
10. Duke, R.M.; Veale, E.B.; Pfeffer, F.M.; Kruger, P.E.; Gunnlaugsson, T. Colorimetric and fluorescent anion sensors: An overview of recent developments in the use of 1,8-naphthalimide-based chemosensors. *Chem. Soc. Rev.* **2010**, *39*, 3936–3953, https://doi.org/10.1039/B910560N.
11. Borges, A.R.; François, L.L.; Welz, B.; Carasek, E.; Vale, M.G.R. Determination of Fluorine in Plant Materials via Calcium Mono-Fluoride Using High-Resolution Graphite Furnace Molecular Absorption Spectrometry with Direct Solid Sample Introduction. *J. Anal. At. Spectrom.* **2014**, *29*, 1564–1569, https://doi.org/10.1039/C4JA00067F.
12. Ozsvath, D.L. Fluoride and Environmental Health: *A Review. Rev. Environ. Sci. Biotechnol.* **2009**, *8*, 59–79. https://doi.org/10.1007/s11157-008-9136-9.
13. Chemchem, M.; Yahaya, I.; Aydıner, B.; Seferoğlu, N.; Doluca, O.; Merabet, N.; Seferoğlu, Z. A Novel and Synthetically Facile Coumarin–Thiophene-Derived Schiff Base for Selective Fluorescent Detection of Cyanide Anions in Aqueous Solution: Synthesis, Anion Interactions, Theoretical Study and DNA-Binding Properties. *Tetrahedron* **2018**, *74*, 6897–6906, http://dx.doi.org/10.1016/j.tet.2018.10.008.
14. Uahengo, V.; Naimhwaka, J.; Daniel, L.S.; Rahman, A.; Elzagheid, M.I.; Rhyman, L.; Ramasami, P.; Cai, P. A Colorimetric Probe for the Real-Time Naked Eye Detection of Cyanide and Hydroxide Ions in Tap Water: Experimental and Theoretical Studies. *Analyst* **2019**, *144*, 6422–6431, https://doi.org/10.1039/C9AN01481K.
15. Yahaya, I.; Chemchem, M.; Aydıner, B.; Seferoğlu, N.; Tepe, F.E.; Açık, L.; Çerçi, N.A.; Türk, M.; Seferoğlu, Z. Novel Fluorescent Coumarin–Thiophene-Derived Schiff Bases: Synthesis, Effects of Substituents, Photophysical Properties, DFT Calculations, and Biological Activities. *J. Photochem. Photobiol. A Chem*. **2019**, *368*, 296–306, https://doi.org/10.1016/j.jphotochem.2018.09.041.
16. Yahaya, I.; Keleş, E.; Putra, A.U.; Yahya, M.; Seferoğlu, N.; Seferoğlu, Z. Microwave-Enhanced and Conventional Procedures for the Synthesis of Coumarin–Thiophene Amides, Sulfonamide, and Urea Derivatives: Synthesis, Photophysical Activities, and Multiple Anion Signaling via Different Mechanisms. *J. Mol. Struct.* **2020**, *1204*, 127465, https://doi.org/10.1016/j.molstruc.2019.127465.
17. Kumar, P.S.; Lakshmi, P.R.; Elango, K.P. Rational Design and Application of a Fluorogenic Chemodosimeter for Selective Detection of Cyanide in an Aqueous Solution via Excimer Formation. *Spectrochim. Acta Part A Mol. Biomol. Spectrosc.* **2019**, *221*, 117172, https://doi.org/10.1016/j.saa.2019.117172.
18. Peng, T.; Li, S.; Zhou, Y.; Liu, R.; Qu, J. Two Cyanoethylene-Based Fluorescence Probes for Highly Efficient Cyanide Detection and Practical Applications in Drinking Water and Living Cells. *Talanta* **2021**, *234*, 122615, https://doi.org/10.1016/j.talanta.2021.122615.
19. Raghavachari, K. Perspective on "Density Functional Thermochemistry. III. The Role of Exact Exchange". *Theor. Chem. Acc.* **2000**, *103*, 361–363, https://doi.org/10.1007/s002149900065.
20. Miehlich, B.; Savin, A.; Stoll, H.; Preuss, H. Results Obtained with the Correlation Energy Density Functionals of Becke and Lee, Yang and Parr. *Chem. Phys. Lett.* **1989**, *157*, 200–206, https://doi.org/10.1016/0009-2614(89)87234-3.
21. Lee, C.; Yang, W.; Parr, R.G. Development of the Colle–Salvetti correlation-energy formula into a functional of the electron density. *Phys. Rev. B* **1988**, *37*, 785, https://doi.org/10.1103/PhysRevB.37.785.
22. Bryantsev, V.S.; Diallo, M.S.; Van Duin, A.C.; Goddard III, W.A. Evaluation of B3LYP, X3LYP, and M06-Class Density Functionals for Predicting the Binding Energies of Neutral, Protonated, and Deprotonated Water Clusters. *J. Chem. Theory Comput.* **2009**, *5*, 1016–1026, https://doi.org/10.1021/ct800549f.
23. Yanar, U.; Babür, B.; Pekyılmaz, D.; Yahaya, I.; Aydıner, B.; Dede, Y.; Seferoğlu, Z. A fluorescent coumarin-thiophene hybrid as a ratiometric chemosensor for anions: Synthesis, photophysics, anion sensing and orbital interactions. *J. Mol. Struct.* **2016**, *1108*, 269–277, https://doi.org/10.1016/j.molstruc.2015.11.081.
24. Yahaya, I.; Seferoğlu, N.; Seferoğlu, Z. Improved One-Pot Synthetic Conditions for Synthesis of Functionalized Fluorescent Coumarin-Thiophene Hybrids: Syntheses, DFT Studies, Photophysical and Thermal Properties. *Tetrahedron* **2019**, *75*, 2143–2154, https://doi.org/10.1016/j.tet.2019.02.034.

25. Minenkov, Y. Solv: An Alternative Continuum Model Implementation Based on Fixed Atomic Charges, Scaled Particle Theory, and the Atom–Atom Potential Method. *J. Chem. Theory Comput.* **2023**, *19*, 5221–5230, https://doi.org/10.1021/acs.jctc.3c00410.
26. Tomasi, J.; Mennucci, B.; Cammi, R. Quantum mechanical continuum solvation models. *Chem. Rev.* **2005**, *105*, 2999–3094, https://doi.org/10.1021/cr9904009.
27. Akonor, B.G.; Aniagyei, A.; Kwawu, C.R.; Amankwah, G.; Menkah, E.S.; Adei, E. A quantum mechanistic investigation into the unusual reactions of nitrilimine and nitrile oxide with 2,3,4,5-tetraphenylcyclopentadienone. *J. Mol. Model.* **2024**, *30*, 282, https://doi.org/10.1007/s00894-024-06074-0.
28. Xu, J.; Carney, T.E.; Zhou, R.; Shepard, C.; Kanai, Y. Real-Time Time-Dependent Density Functional Theory for Simulating Nonequilibrium Electron Dynamics. *J. Am. Chem. Soc.* **2024**, *146*, 5011–5029, https://doi.org/10.1021/jacs.3c08226.
29. Bauernschmitt, R.; Ahlrichs, R. Treatment of electronic excitations within the adiabatic approximation of time dependent density functional theory. *Chem. Phys. Lett.* **1996**, *256*, 454–464, https://doi.org/10.1016/0009-2614(96)00440-X.
30. Frisch, M. Gaussian 09, Revision D.01; Inc.: Wallingford, CT, USA, **2009**.
31. Tawiah, A.; Amankwah, G.; Akonor, B. G.; Adei, E. Deciphering the mechanism and selectivities of the reactions of mesitonitrile oxide with 1,5-dimethyl-6-methylenetricyclo[3.2.1.0^{2,7}]oct-3-en-8-one derivatives: A computational approach. *Comput. Theor. Chem*. **2025**, *1245*, 115093, https://doi.org/10.1016/j.comptc.2025.115093.
32. Romano, G.M.; Savastano, M.; Bazzicalupi, C.; Chelli, R.; Lippolis, V.; Bencini, A. Inorganic anion recognition in aqueous solution by coupling nearby highly hydrophilic and hydrophobic moieties in a macrocyclic receptor. *Dalton Trans.* **2023**, *52*, 6457–6472, https://doi.org/10.1039/D3DT00682D.
33. Mansha, M.; Khan, S.A.; Aziz, M.A.; Khan, A.Z.; Ali, S.; Khan, M. Optical Chemical Sensing of Iodide Ions: A Comprehensive Review for the Synthetic Strategies of Iodide Sensing Probes, Challenges, and Future Aspects. *The Chemical Record* **2022**, *22*, e202200059, https://doi.org/10.1002/tcr.202200059.
34. Wu, Y.; Zhang, Y.; Li, X.; Liu, Y. The Colorimetric Sensor Based on Azobenzenes with Sulfonamide Group for Fluorine Ion and Moisture Detection in Organic Solvents. *Chem. Select* **2022**, *7*, e202200992, https://doi.org/10.1002/slct.202200992.
35. Ranolia, A.; Bala, I.; Jangir, J.; Singh, S.; Sindhu, J.; Kumar, P.; Singh, D. Rationally Designed Dual-Channel Reversible Probe for Cyanide Recognition in Aqueous Medium with Solid-State Sensing Abilities. *J. Photochem. Photobiol. A Chem.* **2024**, *453*, 115650, https://doi.org/10.1016/j.jphotochem.2024.115650.
36. Seferoğlu, Z.; Yahaya, I. Fluorescence Dyes for Determination of Cyanide. In Photochemistry and Photophysics - Fundamentals to Applications, Saha, S., Mondal, S., Eds.; IntechOpen: Rijeka, **2018**; https://doi.org/10.5772/intechopen.75090.
37. Wang, Y.; Wang, Y.; Guo, F.; Wang, Y.; Xie, P. A New Naked-Eye Fluorescent Chemosensor for Cu(II) and Its Practical Applications. *Res. Chem. Intermed.* **2021**, *47*, 3515–3528, https://doi.org/10.1007/s11164-021-04489-5.
38. Jia, X.; Yang, Y.; He, Y.; Ma, Q.; Liu, Y. Theoretical Study on the Sensing Mechanism of a Fluorescence Chemosensor for the Cyanide Anion. Spectrochim. *Acta Part A Mol. Biomol. Spectrosc.* **2019**, *216*, 258–264, https://doi.org/10.1016/j.saa.2019.03.034.
39. Zhong, L.; Li, H.; Wang, S.-L.; Song, Q.-H. The sensing property of charge-transfer chemosensors tuned by acceptors for colorimetric and fluorometric detection of CN^-/HCN in solutions and in gas phase. *Sensors Actuators B Chem.* **2018**, *266*, 703–709, https://doi.org/10.1016/j.snb.2018.03.025.

Publisher's Note & Disclaimer

Supplementary materials

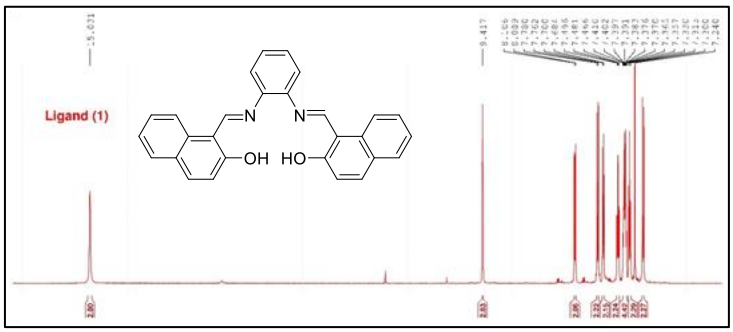

Figure S1. ^{1}H NMR spectrum of **DiNa**.

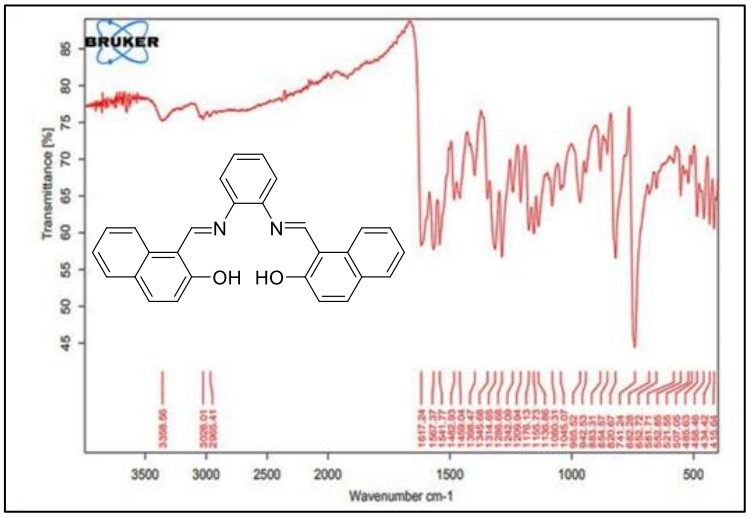

Figure S2. FT-IR spectrum of **DiNa**.

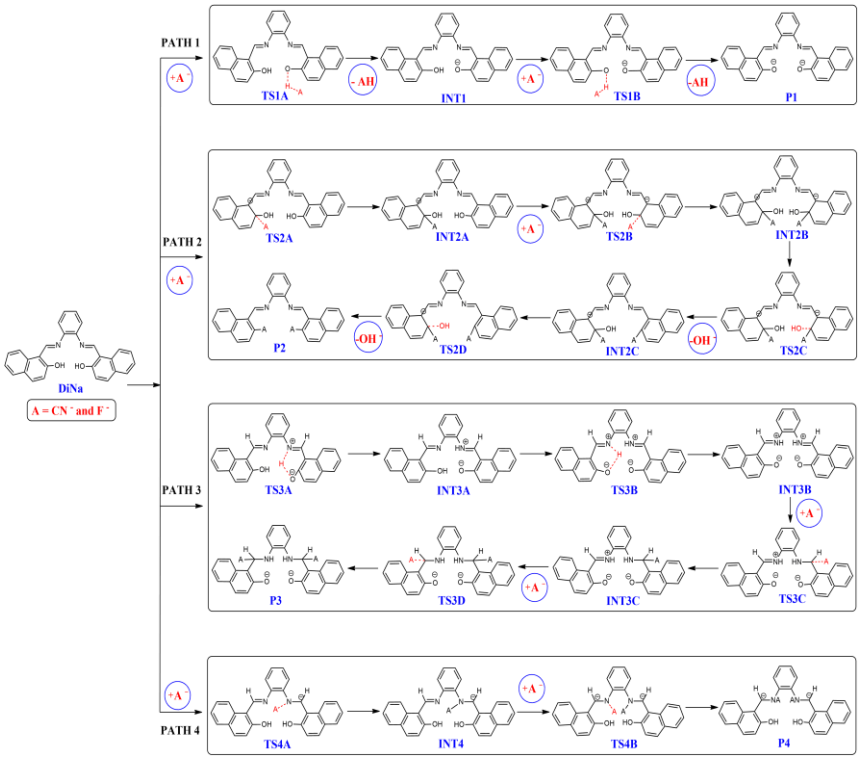

Figure S3. Proposed sensing mechanism for the various anions (CN^{-}, F^{-}) by **DiNa**.